Batteries Hot Paper

How to cite: *Angew. Chem. Int. Ed.* **2020**, *59*, 11483–11490
International Edition: doi.org/10.1002/anie.202002560
German Edition: doi.org/10.1002/ange.202002560

Multi-Electron Reactions Enabled by Anion-Based Redox Chemistry for High-Energy Multivalent Rechargeable Batteries

Zhenyou Li, Bhaghavathi P. Vinayan, Piotr Jankowski, Christian Njel, Ananyo Roy, Tejs Vegge, Julia Maibach, Juan Maria García Lastra, Maximilian Fichtner, and Zhirong Zhao-Karger**

Abstract: *The development of multivalent metal (such as Mg and Ca) based battery systems is hindered by lack of suitable cathode chemistry that shows reversible multi-electron redox reactions. Cationic redox centres in the classical cathodes can only afford stepwise single-electron transfer, which are not ideal for multivalent-ion storage. The charge imbalance during multivalent ion insertion might lead to an additional kinetic barrier for ion mobility. Therefore, multivalent battery cathodes only exhibit slope-like voltage profiles with insertion/extraction redox of less than one electron. Taking VS_4 as a model material, reversible two-electron redox with cationic–anionic contributions is verified in both rechargeable Mg batteries (RMBs) and rechargeable Ca batteries (RCBs). The corresponding cells exhibit high capacities of $>300\ mAh\,g^{-1}$ at a current density of $100\ mA\,g^{-1}$ in both RMBs and RCBs, resulting in a high energy density of $>300\ Wh\,kg^{-1}$ for RMBs and $>500\ Wh\,kg^{-1}$ for RCBs. Mechanistic studies reveal a unique redox activity mainly at anionic sulfides moieties and fast Mg^{2+} ion diffusion kinetics enabled by the soft structure and flexible electron configuration of VS_4.*

[*] Dr. Z. Li, Dr. B. P. Vinayan, A. Roy, Prof. M. Fichtner, Dr. Z. Zhao-Karger
Helmholtz Institute Ulm (HIU) Electrochemical Energy Storage
Helmholtzstrasse 11, 89081 Ulm (Germany)
E-mail: zhenyou.li@kit.edu
zhirong.zhao-karger@kit.edu
Dr. P. Jankowski, Prof. T. Vegge, Prof. J. M. G. Lastra
Department of Energy Conversion and Storage, Technical University of Denmark (DTU)
Anker Engelunds Vej, 2800 Kgs. Lyngby (Denmark)
Dr. C. Njel, Dr. J. Maibach
Institute for Applied Materials (IAM), Karlsruhe Institute of Technology (KIT)
Hermann-von-Helmholtz-Platz 1, 76344 Eggenstein-Leopoldshafen (Germany)
Prof. M. Fichtner
Institute of Nanotechnology (INT), Karlsruhe Institute of Technology (KIT)
Hermann-von-Helmholtz-Platz 1, 76344 Eggenstein-Leopoldshafen (Germany)
Supporting information and the ORCID identification number(s) for the author(s) of this article can be found under: https://doi.org/10.1002/anie.202002560.

Introduction

The increasing demand for electrochemical energy-storage devices with higher energy density has aroused extensive interest in developing multivalent battery systems as they could potentially provide high capacity.[1] Magnesium is an abundant, environmentally benign element, which exhibits non-dendritic nature during electrochemical plating. It has been considered as an ideal option among the multivalent metals when integrated as an anode in rechargeable batteries.

To utilize the advantages of Mg, the high charge density of the Mg^{2+} ion, which usually leads to low diffusion kinetics in the solid hosts, needs to be overcome. As a result, most of the conventional cathodes used for Li ion batteries (LIBs) or their Mg-substituted analogues including transition-metal oxides and polyanion compounds have been shown to be less effective for Mg insertion. Recently, much effort has been made to establish novel intercalation chemistries based on, for example, hydrated Mg^{2+} ion,[2] solvated Mg^{2+} ion,[3] or $MgCl^{+}$ ion[4] shuttle, for rechargeable Mg batteries (RMBs), aiming at shielding the strong electrostatic interaction between the Mg-ion and the host. Improved diffusion kinetics have been clarified through the design of the intercalation cation species. However, the corresponding charge–discharge profiles in practical cells still suffer from slope-like features with limited energy density, which is different from their Li^{+} ion or Na^{+} ion storage behaviours.

As well as the intrinsic high charge density, Mg^{2+} ion storage also requires a local di-electron or multi-electron transfer to compensate their double charge. However, this criterion has not yet attracted sufficient attention when screening the cathodes. In fact, multiple electron redox reactions can be achieved in classical Li-ion insertion cathodes that rely on cationic redox, but only by stepwise single-electron transfer reactions of the transition metals.[5] This charge storage mechanism seems more difficult for divalent ions storage as they might have to adjust their configuration and be stored in a shared position between neighbouring redox centres to balance the double charge, which would set up additional roadblocks for Mg^{2+} ion diffusion besides the strong electrostatic interaction with the host matrix. So far, there are few reports about insertion cathodes, which reversibly host Mg^{2+} ions with more than one electron transfer per redox centre.[6] In this sense, the discovering of a cathode that undergoes reversible two-electron (or multi-electron) redox reactions is particularly important yet challenging for Mg batteries.

The difficulties with the conventional intercalation chemistry for multivalent ions directs research activities toward exploring novel charge storage mechanisms, which could fulfil the requirements for a multivalent battery. Recently, electrode materials based on multi-electron redox reactions have attracted considerable attention for LIBs owing to their potential for a multi-fold increase in capacity by storing multiple monovalent Li-ions. A renowned example is Li-rich oxides with unexpected high capacity, which is attributed to the anionic redox of $O^{2-}/(O_2)^{n-}$.[7] In addition, transition metal polyphosphides[8] and transition-metal polysulfides (TMPs)[9] also undergo multi-electron redox reactions at their anion centres. Given the flexible charge transfer nature, insertion cathodes utilizing anionic redox could be a more feasible option for multivalent ion storage compared to those cationic redox-based materials. However, little attention has been paid to the anionic intercalation redox chemistry for multivalent batteries, though the anion contribution was already elucidated in the reversible Mg-ion intercalation into Chevrel phase Mo_6S_8.[10]

Hammouri's group[11] and Takagi's group[12] first reported anion involved redox reactions of titanium trisulfide (TiS_3) in RMBs by theoretical calculation and experiment, respectively, but with limited capacity and cycling stability. A recent study on vanadium tetrasulfide (VS_4) showed improved capacity and promising cycling stability using 2 PhMgCl-$AlCl_3$ electrolyte.[13] However, in this work only around 0.5 Mg^{2+} ion per formula could be reversibly accommodated in the host. Besides, more information is needed to clarify the redox mechanism.[13]

The electrolyte is also a crucial factor determining the reversibility and accessible energy of multivalent batteries. In fact, recent studies have identified monovalent $MgCl^+$ ion insertion in both inorganic and organic cathodes from the prevalent Cl-based electrolytes in RMBs, leading to lower specific energies of the Mg cells as expected.[4,14] Taking this into account, Cl-free electrolytes, such as magnesium tris(2H-hexafluoroisopropyl) borate,[15] magnesium monocarborane,[16] magnesium perfluorinated pinacolatoborate,[17] and magnesium tetrakis(hexafluoroisopropyloxy)borate ($Mg[B(hfip)_4]_2$),[18] which contain solely Mg-ions as charge carrier, could be an optimal option for studying Mg-ion insertion chemistry. Moreover, the high oxidative stability, high ionic conductivity and non-corrosive properties render this borate electrolyte well suitable for practical application in Mg batteries.[19] Very recently, we have developed the calcium analogue compound, that is, calcium tetrakis(hexafluoroisopropyloxy)borate ($Ca[B(hfip)_4]_2$) for use as Ca electrolyte. It fulfils most of the requirements as a practical electrolyte for Ca batteries.[20]

Herein, we investigated VS_4 as an insertion cathode based on anion based redox reactions for both rechargeable Mg and Ca batteries (RMBs and RCBs) using these new borate electrolytes, respectively. Besides its high theoretical capacity, the flexible quasi one-dimensional (1D) molecular structure of patronite VS_4 and the chemical softness of the sulfides can be particularly favourable for the diffusion of multivalent ions.[21] In addition, VS_4 possesses a semi-conductive nature with a small band gap of only around 1.0 eV,[9b] which is beneficial for electron transfer, as well. We present a comprehensive mechanistic and theoretical study that reveals that VS_4 undergoes interesting anionic redox reactions in Mg and Ca based batteries. Different from the typical cationic redox reactions, such anionic redox chemistry not only shows enhanced kinetics, but also enables reversible multi-electron redox chemistry, which is proven an effective approach towards high-energy multivalent battery systems.

Results and Discussion

Patronite VS_4 has a monoclinic prismatic crystal structure composed of parallelly aligned molecular chains as shown in Figure 1 a. The S atoms in VS_4 exist in the form of $(S–S)^{2-}$ dimer bridging two adjacent V atoms and extending along the *c*-axis.[22] In contrast to the conventional rigid inorganic structures compounds with strong ionic bonds, the relatively large inter-chain distance of 5.83 Å suggests that VS_4 chains are held by relatively weak van der Waals forces, which provides a loosely packed soft structure beneficial for ion diffusion. The 1D feature of the VS_4 chains could be potentially beneficial for maintaining the structural stability during electrochemical processes.

VS_4 was synthesized hydrothermally in the presence of graphene oxide (GO). According to a previous study, the large graphitic regions (surface area) and well dispersion of the GO substrate could promote the conversion of VS_2 to VS_4 efficiently.[9b] X-ray diffraction (XRD) patterns of the resultant VS_4/rGO powder shown in Figure 1 b indicate the main phase to be patronite VS_4 according to the standard pattern

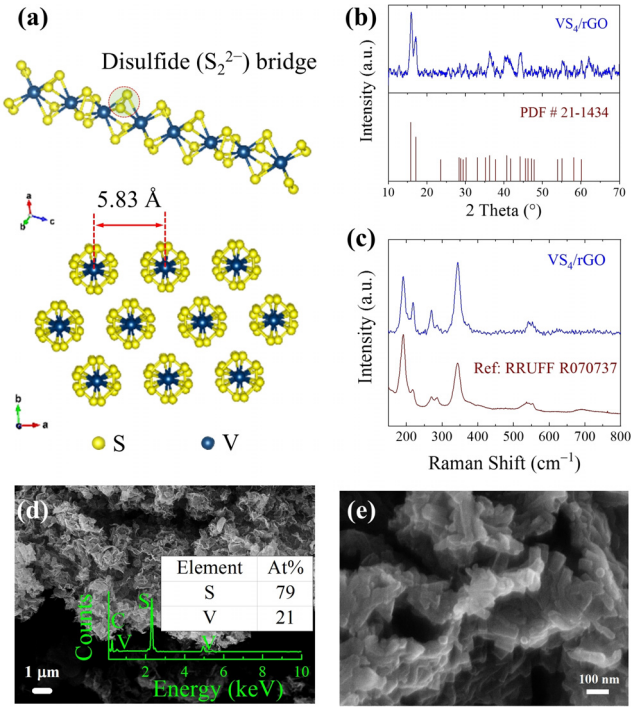

Figure 1. Morphology and structural characterizations of VS_4/rGO. a) Molecular structure; b) powder XRD; c) Raman; d) SEM image with EDX spectrum; e) SEM image with a higher magnification.

(PDF card No. 21-1434). There are two prominent diffraction peaks at 15.8° and 17.1°, which are attributed to (110) and (020) planes of VS_4, respectively, indicating a preferred growth along the c-direction. The absence of characteristic peaks for carbon at 20–30° is a result of the low carbon content in the composite. The carbon content was examined by thermogravimetric analysis coupled with differential scanning calorimetry (TGA-DSC) in flowing air. Two exothermic peaks were recorded in the DSC curve correlating to the oxidation of VS_4 and rGO, respectively. The rGO content was accordingly determined to be approximately 8 wt% (Figure S1 in the Supporting Information). The molecular structure of the VS_4/rGO was characterized by Raman spectroscopy (Figure 1c). All the Raman modes can be well indexed by a VS_4 reference from the RRUFF database (R070737). The peaks at 191 cm^{-1} and 219 cm^{-1} correspond to the V–S stretching mode. The signal at 343 cm^{-1} is attributed to the V_2S_4-cage breathing. While the modes at 271 cm^{-1}, 285 cm^{-1}, and 540–550 cm^{-1} are indicative of S–S bond stretching and twisting from the S_2^{2-} group.[21,23]

Morphological study of VS_4/rGO reveals flower-like agglomerates of VS_4 nanosheets (Figure 1d). However, the nanosheets are not the primary particles. Instead, they are assembled from VS_4 nanorods approximately 60 nm in diameter and several hundred nm long, which confirms the epitaxial growth along the *c*-axis. The EDX spectrum in the inset of Figure 1d indicates C, V, and S in the composite with a V/S ratio of around 1:4, which is consistent with the stoichiometric ratio of VS_4.

The electrochemical properties of VS_4/rGO cathode were first investigated by cyclic voltammetry (CV) with a three-electrode cell setup. In the initial anodic scan, a reduction peak at 0.82 V is present as shown in Figure 2a, suggesting the magnesiation reaction of the VS_4 electrode. The reduction peak shifts to a higher voltage of 1.02 V with a shoulder peak at 1.16 V in the following cycles. A new peak at 1.58 V also appears from the second cycle onwards. The emerging new peaks could be related to the formation of a new intermediate phase,[24] while the peak shift might be attributed to the structural rearrangement due to compositional changes,[25] which might further facilitate Mg^{2+} ion diffusion. In the cathodic scans, the corresponding oxidation peaks with current responses are shown at 1.51 V, 1.79 V, and 1.89 V, respectively, indicating reversible de-/magnesiation processes.

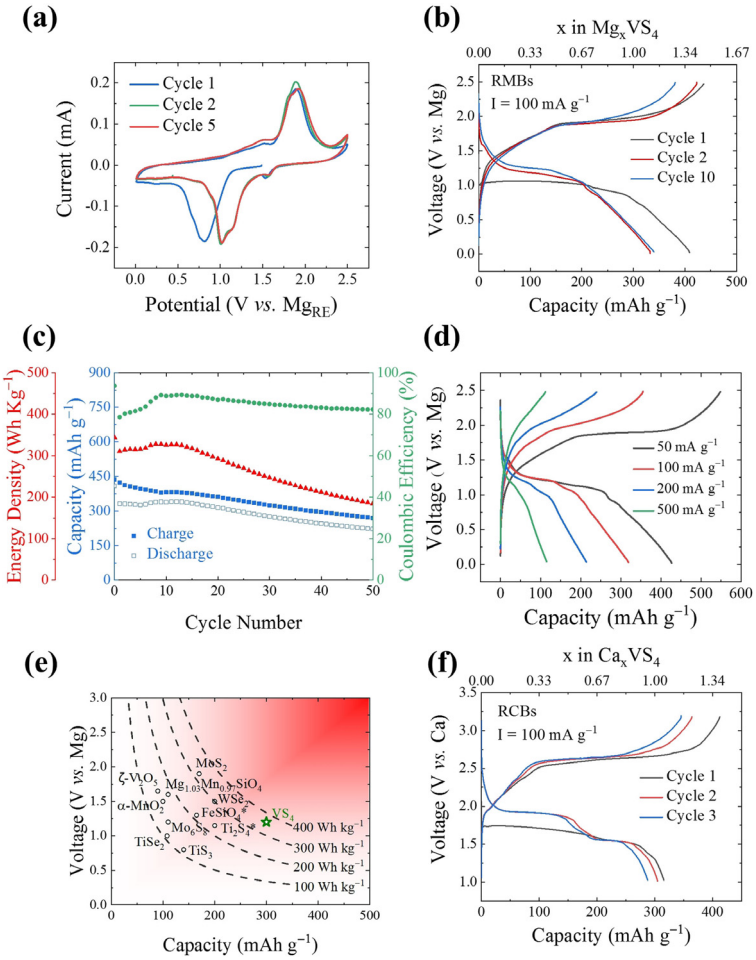

Figure 2. Electrochemical performance of the VS_4/rGO cathode. a) CV curves of VS_4/rGO electrode versus Mg reference (Mg_{RE}) at a scan rate of 0.1 mV s^{-1}. b) Typical charge–discharge profiles and c) cycling stability of VS_4/rGO in the Mg cells at 100 mA g^{-1}. d) Voltage profiles of VS_4/rGO cathode at different current densities. e) VS_4/rGO and other insertion cathodes for RMBs in terms of the voltage and specific capacity. Detailed data used for this chart can be found in Table S1. f) Charge–discharge profiles of VS_4/rGO in the first three cycles at 100 mA g^{-1} in the Ca cells.

The reversibility of the redox reactions is also demonstrated in the galvanostatic measurements. Figure 2b exhibits typical voltage profiles of VS_4/rGO in RMBs at a current rate of 100 mA g^{-1}. A discharge plateau at about 1.0 V was observed in the first cycle, which shifted to a higher voltage of around 1.2 V in the following cycles. In the charging process, the corresponding voltage plateau appears at around 1.8 V after a slope from 1.3 V. All main features in the charge–discharge curves match well with the CV data. The cell delivered an initial capacity of 408 mAh g^{-1}, corresponding to insertion of approximately 1.35 Mg^{2+} ions into one formula of VS_4. Accordingly, the magnesiation of VS_4 involves nearly three-electron transfer per VS_4 unit.

The cell could retain a capacity of 300–350 mAh g^{-1} for up to 25 cycles as shown in Figure 2c. It is still associated to more than one Mg^{2+} ion storage, which suggests reversible multi-electron redox reactions of VS_4 in Mg-based systems. However, the system provides a relatively low coulombic efficiency of around 120%, which might be attributed to some Mg residues in the VS_4 structure during cycling. Another possible reason would be a structural degradation during continuous de-/magnesiation, leading to a loss of the active material. Experimental evidence of the degradation will be presented in the mechanism investigation part. Upon extended cycling, a slow decrease in capacity was observed and approximately 200 mAh g^{-1} remained after 50 cycles. Based on the capacity and voltage values, VS_4/rGO cathodes can provide a high energy density of over 300 Wh Kg^{-1} at a power density of approximately 100 W kg^{-1}.

Furthermore, the rate performance of the VS_4/rGO cathode was also studied. As presented in Figure 2d, the VS_4/rGO cathode delivered a high capacity of 440 mAh g^{-1} at a current rate of 50 mA g^{-1} and a capacity retention of 119 mAh g^{-1} at a high current rate of 500 mA g^{-1}, respectively. Meanwhile, the charge–discharge plateaus are still identifiable at the high currents, which implies a fast mobility of Mg-ions. With the fast Mg kinetics, long-term cycling stability of VS_4/rGO cathodes was tested at 500 mA g^{-1}, demonstrating a lifespan of over 350 cycles (Figure S2). In comparison with other reported insertion-type cathodes, VS_4/rGO represents the state-of-the-art cathode for RMBs in terms of both energy and power density (Figure 2e).

Encouraged by the promising results of VS_4 in Mg system, we also examined the feasibility of this type of multi-electron reaction in a Ca based system. With the recent progress on Ca borate electrolyte,[20] we were able to validate this concept by coupling VS_4 with a Ca anode. With the same current density of 100 mA g^{-1}, a similar trend was observed in the charge–discharge profile of VS_4/rGO cathode in RCBs (Figure 2f). In the first cycle, the discharge plateau displays at 1.7 V, delivering a capacity of 315 mAh g^{-1}. Similar to the Mg based system, the discharge plateau emerges at an elevated voltage of approximately 2.0 V from the second cycle, which might be attributed to the formation of fresh and reactive Ca deposits during the first charging process. In general, owing to the lower standard reductive potential of Ca metal, the Ca cell exhibits higher discharge voltage compared to those of the Mg cells. The VS_4/rGO cathode provided a capacity of around 300 mAh g^{-1} in the initial cycles, which is associated with the accommodation of around 1 Ca^{2+} ion per VS_4 formula. As a result, the cell could offer a promising high energy density of >500 Wh kg^{-1}. However, the cycling stability of the VS_4-based Ca cell was inferior to the Mg system as shown in Figure S4. Further improvement of the Ca batteries is under investigation.

To investigate the Mg storage mechanism, structural analysis including ex situ XRD and operando Raman spectroscopy were performed. The electrode samples for the post mortem studies were collected after the 2nd cycle. As shown in Figure 3a, the characteristic XRD reflections for VS_4 at 16–18° were maintained at all selected states of charge. (The peaks at 43° and 51° are attributed to the stainless steel (SS) current collector as shown in Figure S5) No obvious shift of (110) and (020) peaks was observed at both discharge and charge states, which implies a negligible volume change during electrochemical de-/insertion of Mg^{2+} ion. Instead, a decrease in the peak intensity can be clearly seen in the diffractograms of all the cycled samples when compared to the one at open circuit voltage (OCV) state. The reduction of peak intensity after cycling is most probably related to the adjustment or rearrangement of the lattice during the initial Mg^{2+} ions insertion. However, there is no obvious difference in the peak intensity upon charging and discharging (in the 2nd cycle), implying a reversible de-/magnesiation processes.

The chemical structure of VS_4/rGO electrode during the electrochemical processes was studied by *operando* Raman spectroscopy. Figure 3b,c presents the Raman spectra of the electrode materials obtained at different electrochemical stages in the 2nd cycle. Compared with the pristine state, all peak positions for the different Raman modes of VS_4, including the V-S stretching mode (193 cm^{-1} and 220 cm^{-1}), S–S stretching from the S_2^{2-} group (272 cm^{-1}), and V_2S_4-cage breathing (347 cm^{-1}) remained unchanged during cycling. At the same time, the intensity of all peaks gradually decreases during discharge and recovers in the corresponding charging state. The fluctuation of the peak intensity could be ascribed to a slight structural distortion or strain induced in the lattice during the Mg-ion insertion. These features confirm the good structural maintenance of VS_4 during the reversible magnesiation and de-magnesiation reactions.

To further investigate the Mg^{2+} ion insertion mechanism, XPS spectra of VS_4/rGO electrodes were recorded at various states of charge. In the survey spectra (Figure S7), Mg peaks (both Mg1s and the Auger peaks MgKLL) start to appear when discharging the cell. The peak intensity reaches its maximum at the fully discharged state (0.01 V) but decreases to a lower value at fully charged state (2.5 V), indicating a reversible Mg^{2+} ion storage in the VS_4 structure. The observation of Mg peaks even at fully charged state indicates that some Mg^{2+} ions may be trapped in the matrix, which is responsible for the coulombic efficiency of the cell exceeding 100% in Figure 2c. The partially irreversibility might result from a kinetic issue due to the Mg–S interaction as observed in the S spectra. Similar issue has also been reported in Mg–S batteries.[26] In this scenario, an improved Mg storage performance with higher reversibility is expected if further tuning the structure for example, by increasing the contact with carbon species.

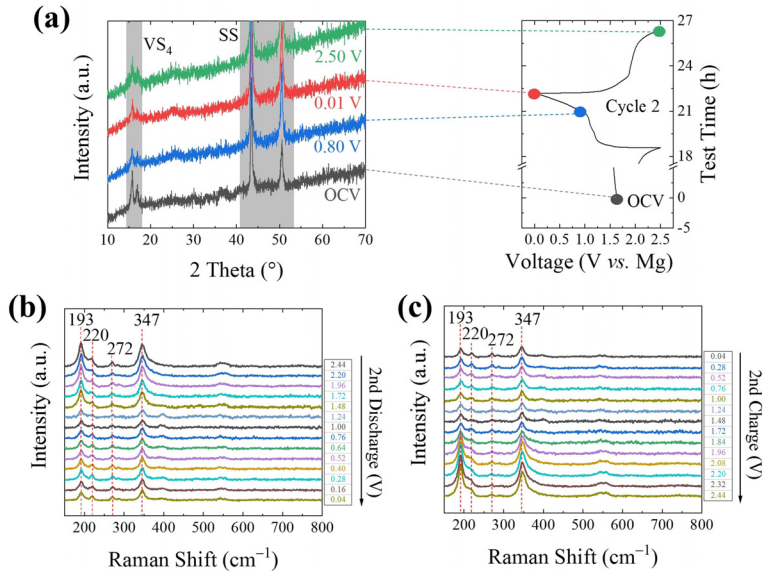

Figure 3. a) Ex situ XRD of the VS_4/rGO cathode at specific states of charge in RMBs. b) and c) show the *operando* Raman spectra of the VS_4/rGO cathode in the 2nd cycle in RMBs.

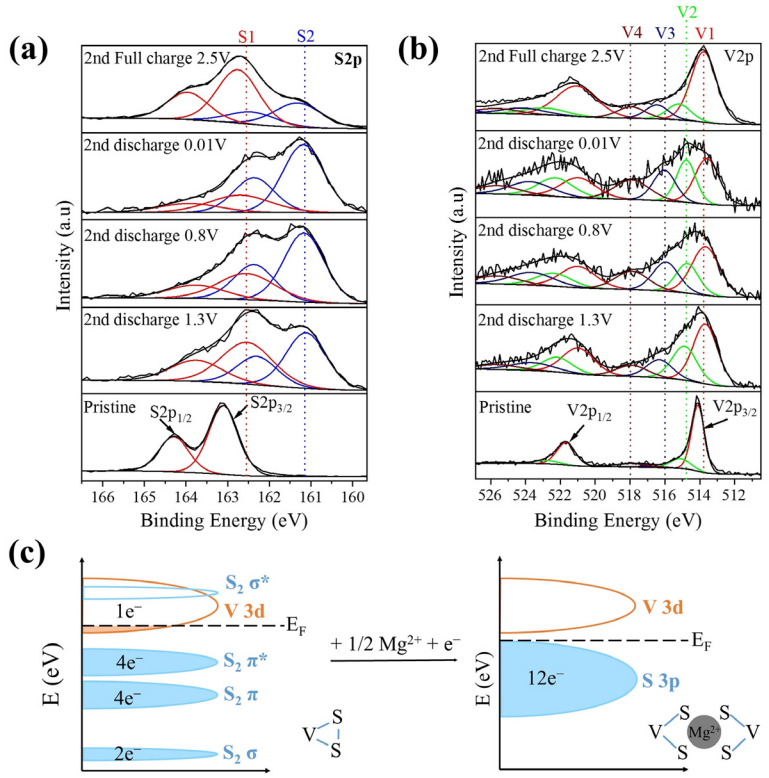

Figure 4. XPS S2p (a) and V2p (b) spectra of the VS_4/rGO electrodes at various states. c) Band structure scheme indicating changes during Mg^{2+} ion insertion.

In the S2p detail spectra (Figure 4a), two peaks corresponding to the characteristic doublet (S1) with a spin orbit splitting of 1.2 eV and an intensity ratio of 2:1 are observed for the pristine electrode. We attribute this S2p ($S2p_{3/2}$ at 163.1 eV) to the S_2^{2-} unit in VS_4.[13] Upon discharging the cell, a new doublet S2 ($2p_{3/2}$ at 161.2 eV) appears, which can be assigned to the S^{2-} species resulting from Mg-S interaction.[13,19] In addition, the peaks for S_2^{2-} species shift to lower binding energy, which could be attributed to the change of the chemical environment of S_2^{2-} due to the presence of more electronegative S1 species and the inserted Mg-ions. The change of the oxidation state of sulfur while accommodating Mg^{2+} ion confirms the occurrence of the redox reactions at the sulfide centre. The variation of the S^{2-}/S_2^{2-} ratio is the

signature of the insertion and de-insertion of Mg^{2+} ions in the host matrix during cycling.

The V 2p spectra were fitted with $2p_{3/2}$–$2p_{1/2}$ doublets separated by 7.6 eV with 2/1 intensity ratio due to spin-orbit coupling. In Figure 4b, the main doublet with $2p_{3/2}$ component at 513.6 eV (V1) is attributed of vanadium–sulfur bond from the VS_4 matrix.[13] As with the sulfur spectra (S1), there is also a shift (−0.5 eV) of the V1 peak to lower binding energies and an increase in full width half maximum (FWHM) during cycling. The three additional doublets V2, V3, and V4 ($2p_{3/2}$ at 515 eV, 516.2 eV, and 518 eV, respectively) are attributed to vanadium with higher oxidation states. The oxidised V2p (V2,V3, V4) peaks are already present in the spectra of all cycled samples and are sensitive to Mg^{2+} ion insertion/extraction in VS_4 structure. Indeed, the peak intensity variation of these compounds is similar to that of S2 species.

The quasi-reversible peak variation present during cycling coupled with the absence of metallic vanadium species suggest that the electrochemical storage of Mg^{2+} ion in the VS_4 host is an insertion type mechanism rather than conversion reactions.[9c,27] The XPS results confirm the Mg^{2+} ion insertion in the VS_4, inducing a cation–anion redox mechanism: oxidation of cationic centre, triggered by reduction of anionic centre.

The hybrid redox mechanism can be explained with the V–S electronic energy band structures. As illustrated in Figure 4c, electronic structure of VS_4 can be simplified as bonding and antibonding orbitals of S_2^{2-}, penetrated by V 3d band. As a result of the energy level ordering, 10 electrons occupy molecular orbitals of disulfide ions (S_2^{2-}), leaving 1 electron at orbital of vanadium (V^{4+}). When a Mg^{2+} cation inserts into the host, it changes the structure of the two S_2^{2-} units. Transferring two electrons to the highly energetic antibonding orbital S_2 σ* would lead to a rather unstable situation and thus it is preferable to break the S–S bonding. After the broken of the S–S bonds, the bonding–antibonding structure of the disulfide 3p orbitals is lost. Instead, a single broad band corresponding to single sulfur ions is formed. The new S 3p band entirely lies below the V 3d band and thus this results in the transfer of electron from vanadium to sulfur, causing observed oxidation of V^{4+} to V^{5+}. This mechanism allows for storage of up to $1.5\,Mg^{2+}$ ion in VS_4 structure, following overall reaction as described in Equation (1):

$$1.5\,Mg^{2+} + 3\,e^- + VS_4[V^{4+},S_2^{2-}] \rightarrow Mg_{1.5}VS_4[V^{5+},S^{2-}] \quad (1)$$

With a flexible electronic configuration, the anionic reactivity in such systems is energetically more favourable for multivalent ion storage compared to other conventional cationic redox reaction based materials. Moreover, such anionic redox reactions can enable multi-electron transfer in electrochemical systems. However, due to the lack of suitable electrolyte that provides dissociated multivalent cation as charge carrier, previous studies on Mg storage in VS_4 could not fulfil the concept. Jin et al.[13] reported VS_4 as promising candidate for RMBs by applying the so-called all-phenyl complex (APC) electrolyte. The cathode exhibited long-term cycling and excellent rate capability, but still limited to approximately $1\,e^-$ transfer during cycling. A follow-up study from Mai's group clarified the $MgCl^+$ storage mechanism in VS_4 structure with APC electrolyte.[28] Rather than Mg^{2+} ions, various $MgCl_x^+$ clusters have been proven to be the active species in nearly all the Cl-based electrolyte systems.[29] The unexpected low capacity is most probably related to the monovalent $MgCl^+$ cation storage into the VS_4 structure. The disulfide group (S_2^{2-}) in VS_4 is capable of receiving two electrons, which eliminates the abovementioned configuration issue of Mg^{2+} ion in classical cationic redox hosts. Whereas, taking up two monovalent ion at one redox site would possibly cause steric problem. In this scenario, Cl-free $Mg[B(hfip)_4]_2$ electrolyte is optimal for validating the novel concept and thus provides higher capacity than the Cl-based electrolytes.

To gain more insight into the unique redox mechanism of VS_4, density functional theory (DFT) calculations were performed. When one Mg^{2+} ion is inserted in the host VS_4 lattice, the two most plausible scenarios are either the reduction of one or several V cations (classical cationic redox) or the reduction of a disulfide S_2^{2-} into two S^{2-} ions (anionic redox). As expected from the analysis before, calculations confirm that during insertion of one magnesium ion, two neighbouring S_2^{2-} anions dissociate into four S^{2-} anions (see the Bader charge analysis[30] and the lattice distortion upon Mg insertion in Figure 5a b). This means that the insertion of one Mg ion leads to a four-electron donation to sulfur atoms: two of these four electrons come from the inserted Mg^{2+} cation and another two from V cations that have been oxidized. The donation of charge from V^{4+} to S^{2-} anions is due to generation of new S 3p band (as mentioned above) as well as its higher stabilization by the presence of the neighbouring Mg^{2+} cation. Overall, our theoretical calculation in terms of charge allocation in VS_4 is consistent with the XPS data, confirming an anionic redox dominated hybrid charge storage mechanism.

Furthermore, this dynamic mechanism of transformation from S_2^{2-} to S^{2-} was found to be vital for fast Mg^{2+} ion diffusion in the VS_4 structure: (di)sulfide anions have a possibility to actively support ion transport by flexible adjustment of their position, in a similar way as polymer electrodes. Interestingly, the quasi 1D structure of VS_4 chains is also analogous to chain-like polymers, providing further structural flexibility. Therefore, two Mg^{2+} ion diffusion paths can be elucidated according to the charge allocation results: 1) parallel to VS_4 chains (Figure 5c) and 2) as jumps from one $S_2^{2-}/2\,S^{2-}$ group to another neighbouring (Figure 5d). Based on a nudged elastic band (NEB) analysis, we found that the latter active support from (di)sulfide anions can lower diffusion barrier from 2.16 to 1.50 eV. A more detailed investigation on the dynamic properties of this system, including, for example, the specifics of the electron-transport mechanism[31] and an automated workflow analysis of the Mg-kinetics could shed additional light on this interesting process.

Conclusion

In summary, we have demonstrated a reversible anionic redox chemistry of VS_4-based cathodes for multivalent

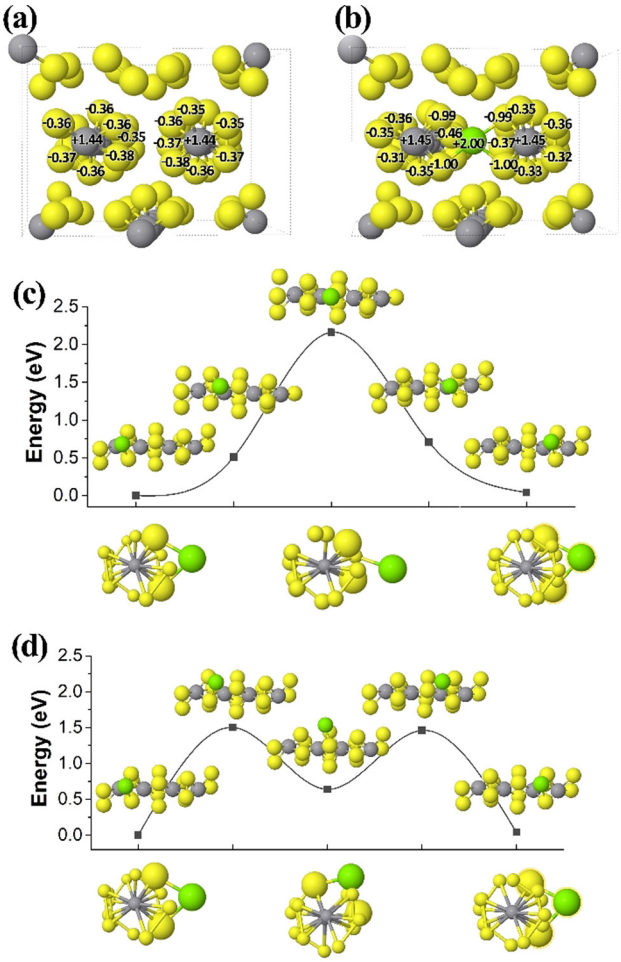

Figure 5. DFT analysis of charge allocation in VS_4 a) before and b) after single Mg^{2+} ion insertion. Energetic profile of Mg^{2+} ion diffusion in VS_4 cathode calculated by a NEB method: c) parallelly to VS_4 chains and d) with jumps between S_2^{2-} anions. One VS_4 chain shown for simplicity of the view.

batteries. Ex situ and operando spectroscopic studies demonstrate the insertion of Mg^{2+} ions and elucidate the anion-dominated redox reactions in the VS_4/rGO cathode. Computational analysis not only confirms the hybrid redox mechanism, but also reveals that the chain-like VS_4 can offer an effective pathway for fast migration of Mg^{2+} ions. The unique charge-storage mechanism based on disulfide anions makes such a material well suited for multivalent-metal-based batteries and capable of multi-electron transfer reaction in RMBs and RCBs, thus providing a high capacity of $>300\ mAh\,g^{-1}$ and a high energy density ($>300\ Wh\,kg^{-1}$ for RMBs and $>500\ Wh\,kg^{-1}$ for RCBs). The strategy involving anionic redox chemistry would provide a new perspective for the development of high performance cathode materials for multivalent batteries.

Acknowledgements

We acknowledge the funding from Bundesministerium für Bildung und Forschung (BMBF) of Germany via the "MagSiMal" project (03XP0208), and from the European Union's Horizon 2020 research and innovation programme under grant agreement No 824066 via the "E-MAGIC" project. This work contributes to the research performed at CELEST (Center for Electrochemical Energy Storage Ulm-Karlsruhe) and was partly funded by the German Research Foundation (DFG) under Project ID 390874152 (POLiS Cluster of Excellence). This work was partly carried out with the support of the Karlsruhe Nano Micro Facility (KNMF, http://www.knmf.kit.edu), a Helmholtz Research Infrastructure at Karlsruhe Institute of Technology (KIT, http://www.kit.edu).

Conflict of interest

The authors declare no conflict of interest.

Keywords: anions · magnesium-ion batteries · multi-electron reactions · rechargeable calcium batteries · VS_4

[1] a) D. Aurbach, Z. Lu, A. Schechter, Y. Gofer, H. Gizbar, R. Turgeman, Y. Cohen, M. Moshkovich, E. Levi, *Nature* **2000**, *407*, 724–727; b) H. D. Yoo, I. Shterenberg, Y. Gofer, G. Gershinsky, N. Pour, D. Aurbach, *Energy Environ. Sci.* **2013**, *6*, 2265–2279.
[2] K. W. Nam, S. Kim, S. Lee, M. Salama, I. Shterenberg, Y. Gofer, J.-S. Kim, E. Yang, C. S. Park, J.-S. Kim, S.-S. Lee, W.-S. Chang, S.-G. Doo, Y. N. Jo, Y. Jung, D. Aurbach, J. W. Choi, *Nano Lett.* **2015**, *15*, 4071–4079.
[3] Z. Li, X. Mu, Z. Zhao-Karger, T. Diemant, R. J. Behm, C. Kübel, M. Fichtner, *Nat. Commun.* **2018**, *9*, 5115.
[4] a) H. D. Yoo, Y. Liang, H. Dong, J. Lin, H. Wang, Y. Liu, L. Ma, T. Wu, Y. Li, Q. Ru, Y. Jing, Q. An, W. Zhou, J. Guo, J. Lu, S. T. Pantelides, X. Qian, Y. Yao, *Nat. Commun.* **2017**, *8*, 339; b) H. Dong, Y. Liang, O. Tutusaus, R. Mohtadi, Y. Zhang, F. Hao, Y. Yao, *Joule* **2019**, *3*, 782–793.
[5] D. H. Evans, *Chem. Rev.* **2008**, *108*, 2113–2144.
[6] M. S. Whittingham, C. Siu, J. Ding, *Acc. Chem. Res.* **2018**, *51*, 258–264.
[7] M. Sathiya, G. Rousse, K. Ramesha, C. P. Laisa, H. Vezin, M. T. Sougrati, M. L. Doublet, D. Foix, D. Gonbeau, W. Walker, A. S. Prakash, M. Ben Hassine, L. Dupont, J. M. Tarascon, *Nat. Mater.* **2013**, *12*, 827.
[8] J. Cabana, L. Monconduit, D. Larcher, M. R. Palacín, *Adv. Mater.* **2010**, *22*, E170–E192.
[9] a) S. S. Zhang, *J. Mater. Chem. A* **2015**, *3*, 7689–7694; b) C. S. Rout, B.-H. Kim, X. Xu, J. Yang, H. Y. Jeong, D. Odkhuu, N. Park, J. Cho, H. S. Shin, *J. Am. Chem. Soc.* **2013**, *135*, 8720–8725; c) S. Britto, M. Leskes, X. Hua, C.-A. Hébert, H. S. Shin, S. Clarke, O. Borkiewicz, K. W. Chapman, R. Seshadri, J. Cho, C. P. Grey, *J. Am. Chem. Soc.* **2015**, *137*, 8499–8508.
[10] J. Richard, A. Benayad, J. F. Colin, S. Martinet, *J. Phys. Chem. C* **2017**, *121*, 17096–17103.
[11] M. Arsentev, A. Missyul, A. V. Petrov, M. Hammouri, *J. Phys. Chem. C* **2017**, *121*, 15509–15515.
[12] K. Taniguchi, Y. Gu, Y. Katsura, T. Yoshino, H. Takagi, *Appl. Phys. Express* **2015**, *9*, 011801.
[13] Y. Wang, Z. Liu, C. Wang, X. Yi, R. Chen, L. Ma, Y. Hu, G. Zhu, T. Chen, Z. Tie, J. Ma, J. Liu, Z. Jin, *Adv. Mater.* **2018**, *30*, 1802563.

[14] C. Pei, Y. Yin, R. Sun, F. Xiong, X. Liao, H. Tang, S. Tan, Y. Zhao, Q. An, L. Mai, *ACS Appl. Mater. Interfaces* **2019**, *11*, 31954 – 31961.
[15] Z. Zhang, Z. Cui, L. Qiao, J. Guan, H. Xu, X. Wang, P. Hu, H. Du, S. Li, X. Zhou, S. Dong, Z. Liu, G. Cui, L. Chen, *Adv. Energy Mater.* **2017**, *7*, 1602055.
[16] O. Tutusaus, R. Mohtadi, T. S. Arthur, F. Mizuno, E. G. Nelson, Y. V. Sevryugina, *Angew. Chem. Int. Ed.* **2015**, *54*, 7900 – 7904; *Angew. Chem.* **2015**, *127*, 8011 – 8015.
[17] J. Luo, Y. Bi, L. Zhang, X. Zhang, T. L. Liu, *Angew. Chem. Int. Ed.* **2019**, *58*, 6967 – 6971; *Angew. Chem.* **2019**, *131*, 7041 – 7045.
[18] Z. Zhao-Karger, M. E. Gil Bardaji, O. Fuhr, M. Fichtner, *J. Mater. Chem. A* **2017**, *5*, 10815 – 10820.
[19] Z. Zhao-Karger, R. Liu, W. Dai, Z. Li, T. Diemant, B. P. Vinayan, C. Bonatto Minella, X. Yu, A. Manthiram, R. J. Behm, M. Ruben, M. Fichtner, *ACS Energy Lett.* **2018**, *3*, 2005 – 2013.
[20] Z. Li, O. Fuhr, M. Fichtner, Z. Zhao-Karger, *Energy Environ. Sci.* **2019**, *12*, 3496 – 3501.
[21] M. S. Weimer, R. F. McCarthy, J. D. Emery, M. J. Bedzyk, F. G. Sen, A. Kinaci, M. K. Y. Chan, A. S. Hock, A. B. F. Martinson, *Chem. Mater.* **2017**, *29*, 2864 – 2873.
[22] R. Allmann, I. Baumann, A. Kutoglu, H. Rösch, E. Hellner, *Naturwissenschaften* **1964**, *51*, 263 – 264.
[23] E. Flores, E. Muñoz-Cortés, J. Bodega, O. Caballero-Calero, M. Martín-González, C. Sánchez, J. R. Ares, I. J. Ferrer, *ACS Appl. Energy Mater.* **2018**, *1*, 2333 – 2340.
[24] A. Yamada, H. Koizumi, S.-i. Nishimura, N. Sonoyama, R. Kanno, M. Yonemura, T. Nakamura, Y. Kobayashi, *Nat. Mater.* **2006**, *5*, 357 – 360.
[25] Y. Zhou, J. Tian, H. Xu, J. Yang, Y. Qian, *Energy Storage Mater.* **2017**, *6*, 149 – 156.
[26] Z. Zhao-Karger, X. Zhao, D. Wang, T. Diemant, R. J. Behm, M. Fichtner, *Adv. Energy Mater.* **2015**, *5*, 1401155.
[27] E. D. Grayfer, E. M. Pazhetnov, M. N. Kozlova, S. B. Artemkina, V. E. Fedorov, *ChemSusChem* **2017**, *10*, 4805 – 4811.
[28] C. Pei, Y. Yin, R. Sun, F. Xiong, X. Liao, H. Tang, S. Tan, Y. Zhao, Q. An, L. Mai, *ACS Appl. Mater. Interfaces* **2019**, *11*, 31954 – 31961.
[29] a) A. Du, Z. Zhang, H. Qu, Z. Cui, L. Qiao, L. Wang, J. Chai, T. Lu, S. Dong, T. Dong, H. Xu, X. Zhou, G. Cui, *Energy Environ. Sci.* **2017**, *10*, 2616 – 2625; b) N. Pour, Y. Gofer, D. T. Major, D. Aurbach, *J. Am. Chem. Soc.* **2011**, *133*, 6270 – 6278; c) M. Salama, I. Shterenberg, L. J. W. Shimon, K. Keinan-Adamsky, M. Afri, Y. Gofer, D. Aurbach, *J. Phys. Chem. C* **2017**, *121*, 24909 – 24918; d) H. S. Kim, T. S. Arthur, G. D. Allred, J. Zajicek, J. G. Newman, A. E. Rodnyansky, A. G. Oliver, W. C. Boggess, J. Muldoon, *Nat. Commun.* **2011**, *2*, 427.
[30] W. Tang, E. Sanville, G. Henkelman, *J. Phys. Condens. Matter* **2009**, *21*, 084204.
[31] H. Park, N. Kumar, M. Melander, T. Vegge, J. M. Garcia Lastra, D. J. Siegel, *Chem. Mater.* **2018**, *30*, 915 – 928.

Manuscript received: February 18, 2020
Accepted manuscript online: March 27, 2020
Version of record online: May 8, 2020

